

Improved microscopic nuclear level densities within the Hartree-Fock-Bogoliubov plus combinatorial method

S. Goriely,^{1,*} S. Hilaire,² and A. J. Koning³¹*Institut d'Astronomie et d'Astrophysique, ULB CP226, B-1050 Brussels, Belgium*²*CEA/DIF, Service de Physique Nucléaire, Boîte Postal 12, F-91680 Bruyères-le-Châtel, France*³*Nuclear Research and Consultancy Group, P.O. Box 25, NL-1755 ZG Petten, The Netherlands*

(Received 4 September 2008; published 15 December 2008)

New developments have been brought to our energy-, spin-, and parity-dependent nuclear level densities based on the microscopic combinatorial model. As in our previous study, a detailed calculation of the intrinsic state density and of the rotational enhancement factor is included, but this time the vibrational contributions explicitly take the phonon excitations into account. The present model predicts the experimental s - and p -wave neutron resonance spacings with a degree of accuracy comparable to that of the best global models available. It is also shown that the model gives a reliable extrapolation at low energies where experimental data on the cumulative number of levels can be extracted. The predictions are also in good agreement with the experimental data extracted from the analysis of particle- γ coincidence in the ($^3\text{He}, \alpha\gamma$) and ($^3\text{He}, ^3\text{He}'\gamma$) reactions. Total as well as partial level densities for more than 8500 nuclei are made available in a table format for practical applications. For the nuclei for which experimental s -wave spacings and enough low-lying states exist, renormalization factors are provided to reproduce simultaneously both observables. The same combinatorial method is used to estimate the nuclear level densities at the fission saddle points of actinides and at the shape isomer deformation. Finally, the new nuclear level densities are applied to the calculation of radiative neutron capture cross sections.

DOI: [10.1103/PhysRevC.78.064307](https://doi.org/10.1103/PhysRevC.78.064307)

PACS number(s): 21.10.Ma, 21.60.Jz

I. INTRODUCTION

Nuclear level densities (NLD) have been a matter of interest and study for years, going back at least to 1936 with Bethe's pioneering work [1]. Since then, more or less sophisticated methods have been developed to reproduce the available experimental data. The so-called partition function method is by far the most widely used technique to calculate level densities, particularly in view of its ability to provide simple analytical formulas. Such a model corresponds to the zeroth-order approximation of a Fermi gas model and leads to very simple analytical, though nonpredictive, expressions for the NLD. In an attempt to reproduce the experimental data, various phenomenological modifications to the original analytical formulation of Bethe have been suggested, in particular to allow for shell, pairing, and collective effects [2–5]. However, drastic approximations are usually made in deriving such analytical NLD formulas and their shortcomings in matching experimental data are overcome by empirical parameter adjustments. The lack of experimental information, in particular at high excitation energies, still constitutes the main problem faced by the NLD models and the parameter-fitting procedures they require, even though the number of analyses of slow neutron resonances and of cumulative numbers of low-energy levels has grown steadily. The most reliable experimental data on NLD concerns the s -wave neutron resonance spacings D_0 at the neutron separation energy S_n . For a nucleus ($Z, A + 1$) resulting from the capture of a low-energy neutron by a target

(Z, A) with spin J_0 and parity P_0 , D_0 is given by

$$D_0 = \frac{1}{\rho(S_n, J_0 + 1/2, P_0) + \rho(S_n, J_0 - 1/2, P_0)} \quad \text{for } J_0 > 0, \quad (1)$$

$$= \frac{1}{\rho(S_n, 1/2, P_0)} \quad \text{for } J_0 = 0.$$

Owing to the low excitation energy S_n at which the level spacing is estimated, D is very sensitive to shell, pairing, and deformation effects. Therefore, systematics based on simple analytical formulas adjusted around this energy, and for stable nuclei only, can lead to large uncertainties, especially when extrapolating to high energies ($U \gtrsim 10$ MeV) or for spins differing from $J_0 \pm 1/2$ and/or to nuclei far from the valley of β -stability.

For specific applications such as nuclear astrophysics or accelerator-driven systems, a large amount of data needs to be extrapolated far away from the experimentally known region. In this case, two major features of the nuclear theory must be contemplated, namely its *reliability* and *accuracy*. A microscopic description by a physically sound model based on first principles ensures a reliable extrapolation away from the experimentally known region. For these reasons, when no experimental data exist to constrain analytical Fermi-gas-type formulas, it is imperative to use preferentially microscopic or semimicroscopic global predictions based on sound and reliable nuclear models, which, in turn, can compete with more phenomenological highly parametrized models in the reproduction of experimental data. Global microscopic models of NLD have been developed in the past decades [6–12], but they are almost never used for practical applications because of their lack of accuracy in reproducing experimental data

*sgoriely@astro.ulb.ac.be

(especially when considered globally on a large data set) or because they do not offer the same flexibility as that of the highly parametrized analytical expressions.

A global microscopic NLD prescription within the statistical approach based on the Hartree-Fock-BCS (HFBCS) ground-state properties [13] has proven the capacity of microscopic models to compete with phenomenological models in the reproduction of experimental data and consequently to be adopted for practical applications. However, this statistical approach presents the drawback of describing neither the parity dependence of the NLD nor the discrete (i.e., nonstatistical) nature of the excited spectrum at low energies. For this reason, we recently improved the combinatorial approach and demonstrated that such an approach can clearly compete with the statistical approach in the global reproduction of experimental data [14]. One of the advantages of this approach is to provide not only the energy, spin, and parity dependence of the NLD but also the partial particle-hole (ph) level density, which cannot be extracted in any satisfactory way from the statistical approaches. At low energies, the combinatorial predictions also provide the nonstatistical limit, where by definition the statistical approach cannot be applied. Our method consists in using the single-particle level scheme obtained from the axially symmetric Hartree-Fock-Bogoliubov (HFB) model to construct incoherent ph state densities as a function of the excitation energy, the spin projection (on the intrinsic symmetry axis of the nucleus), and the parity. Once these incoherent ph state densities are determined, collective rotational effects are included by building up rotational bands consistently. In Ref. [14], the choice was made to describe the vibrational effects by multiplying the total level densities by a phenomenological enhancement factor described in Refs. [4,5]. The resulting NLD were found to reproduce very well the available experimental data (i.e., both the cumulative number of low-energy levels and the s - and p -wave resonances mean spacings at the neutron binding energy). However, it is clear that the phenomenological treatment of vibrational effects needs to be replaced by a sounder treatment. Feedback from fission cross section calculations also suggested the lack of vibrational states at low energies [15].

To improve the reliability of the microscopic prediction of NLD, the vibrational enhancement factor is now included in the combinatorial approach explicitly by allowing for phonon excitations. The formalism is described in Sec. II. The nuclear structure properties obtained within the recent deformed HFB-14 model is briefly described in the same section. The same formalism is also applied to the calculation of NLD at the fission saddle points. In Sec. III, the resulting NLD are compared with experimental data. A possible renormalization of the NLD on such data is proposed. Some applications to reaction cross section calculations are illustrated in Sec. IV. Conclusions are drawn in Sec. V.

II. THE COMBINATORIAL MODEL OF NLD

The microscopic method used to compute NLD is the combinatorial method as described in detail in Refs. [10,11,14]. It consists in using the HFB single-particle level scheme

to construct incoherent ph state densities $\rho_{\text{ph}}(U, M, \pi)$ as a function of the excitation energy U , the spin projection M on the intrinsic symmetry axis of the nucleus, and the parity π . Once these incoherent ph state densities are determined, we account for collective effects to deduce the total level density. In Ref. [14], we made the choice of multiplying the level densities by the phenomenological vibrational enhancement factor after accounting for rotational motion if necessary (i.e., for deformed nuclei). The resulting NLD were found to reproduce rather well the available experimental data (i.e., both the low-energy levels and the s - and p -wave resonance spacings). This phenomenological treatment is now replaced by a sounder treatment.

A. The vibrational enhancement

To treat the phonon excitations explicitly, the vibrational enhancement can be properly described by using a boson partition function [11]. To do so, the phonons' state densities are constructed and folded with the incoherent ph densities. In practice, this means that supplementary low-energy phonon states that were not considered in our previous approach [14] are now included. The construction of the vibrational states follows the method described in Ref. [11], which consists in expanding the generalized boson partition function,

$$\mathcal{Z}_{\text{vib}} = \prod_{\lambda} \prod_{\mu} \sum_{N_{\text{ph}}} [x y^{\varepsilon_{\lambda\mu}} t^{\mu} p_{\lambda}]^{N_{\text{ph}}}, \quad (2)$$

where x , y , and t enable us to keep track of the number of bosons, their excitation energies, and their spin projections, respectively. In this equation, $\varepsilon_{\lambda\mu}$ is the energy of a phonon with multipolarity λ and spin projection μ , and $p_{\lambda} = (-1)^{\lambda}$ or $(-1)^{(\lambda+1)}$ for isoscalar and isovector phonons, respectively. For spherical nuclei, the phonons' energies are $(2\lambda + 1)$ -fold degenerate for a phonon of multipolarity λ , and μ takes on all the integer values between $-\lambda$ and λ . For deformed nuclei, the energies are, in principle, no longer degenerate and some μ values are ruled out for quadrupole modes as a result of symmetries imposed on nuclear shapes and collective wave functions [16]. In practice, this means that only the projections $\mu = 0$ (β vibrations) and ± 2 (γ vibrations) survive for the quadrupole phonons; hence, for $\lambda = 2$, the product over μ in Eq. (2) is restricted to $\mu = -2, 0, \text{ and } 2$. For other multipole modes, all possible μ values are kept since the symmetries imposed on nuclear shapes and collective wave functions are already accounted for.

For the number of coupled phonons, we consider a maximum number of three phonons. Indeed, two-phonon states are well established [17–27], and possible three-phonon states have also been called for [28]. There is however no physical justification for this adopted number. In addition to the quadrupole and octupole vibrational modes, we also include hexadecapole ($\lambda = 4$) modes, since, as initially suggested in Ref. [29], such modes may affect the NLD because of their possibly relatively low excitation energies [30–34], especially in the rare-earth and actinide mass regions. As in our previous study [14], we use a modified shell-dependent systematic of experimental levels interpreted to be quadrupole and octupole

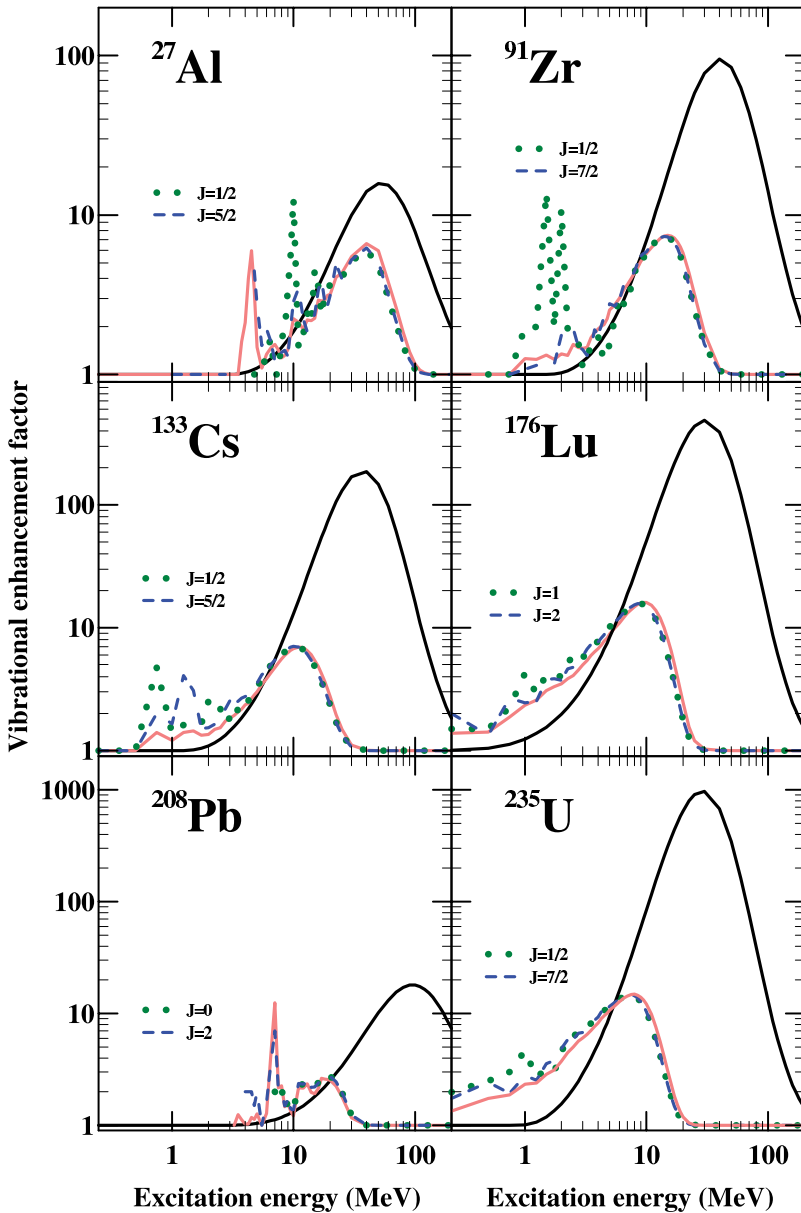


FIG. 1. (Color online) Total (light solid line) and spin-dependent (dashed and dotted lines) vibrational enhancement factor K_{vib} compared to the phenomenological formula (solid black line) adopted in Ref. [14].

vibrational levels to derive an analytical expression for the phonon energies. For quadrupole and octupole modes the analytical expression is the same as in Ref. [14], that is, respectively,

$$\omega_2[\text{MeV}] = 65A^{-5/6}/(1 + 0.05E_{\text{shell}}) \quad (3)$$

and

$$\omega_3[\text{MeV}] = 100A^{-5/6}/(1 + 0.05E_{\text{shell}}). \quad (4)$$

The hexadecapole mode can be expressed relative to the quadrupole mode [4], leading to a similar expression, namely

$$\omega_4[\text{MeV}] = 160A^{-5/6}/(1 + 0.05E_{\text{shell}}). \quad (5)$$

In these expressions, the shell correction energy E_{shell} is determined as explained in Ref. [14]. For practical calculations, experimental data are used whenever available.

As already mentioned, once the vibrational and incoherent ph state densities are computed, they are folded to deduce

the total state and level densities [14]. To account for the damping of vibrational effects at increasing energies, we restrict the folding to the ph configurations having a total exciton number (i.e., the sum of the number of proton and neutron particles and proton and neutron holes) $N_{\text{ph}} \leq 4$. This restriction stems from the fact that a vibrational state results from a coherent excitation of particles and holes and that this coherence vanishes with increasing numbers of particles and holes involved in the description. Therefore, if one deals with a ph configuration having a large exciton number, one should not simultaneously account for vibrational states that are clearly already included as incoherent excitations.

The resulting vibrational enhancement factor K_{vib} (corresponding to the ratio of the NLD including phonon excitations to those neglecting them) is illustrated for a sample of nuclei in Figs. 1 and 2. The microscopic character of our new treatment is seen to give rise to an oscillating energy dependence, in

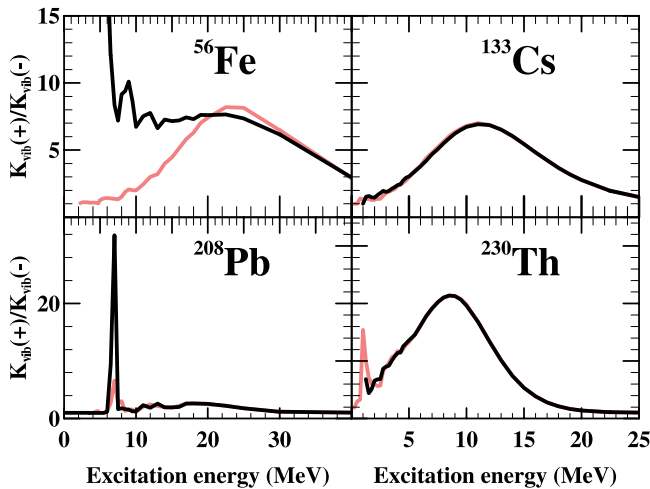


FIG. 2. (Color online) Vibrational enhancement factor K_{vib} for positive (light curve) and negative (black curve) parities.

contrast to the smooth behavior of the temperature-dependent expression [4,5]. The enhancement factor K_{vib} is clearly spin- and parity-dependent. In addition, the present approach allows for a description of the existence of vibrational states at very low energy within the so-called pairing gap where no ph excitations are possible yet. This pure boson state density cannot be described when simply including a multiplying enhancement factor to the intrinsic NLD and can play an important role in fission cross section calculations.

The prescription adopted here also leads to a damping of K_{vib} at lower energies in comparison with the phenomenological approach [14]. Finally, for nuclei having many low-energy vibrational levels (e.g., ^{238}U), the new enhancement factor departs from unity at much lower energy than with the analytical approximation.

In addition to the state densities, the partial level densities can also play an important role in the reaction model, mostly in the description of the pre-equilibrium reaction mechanism within the so-called exciton model (see Refs. [35–37] for

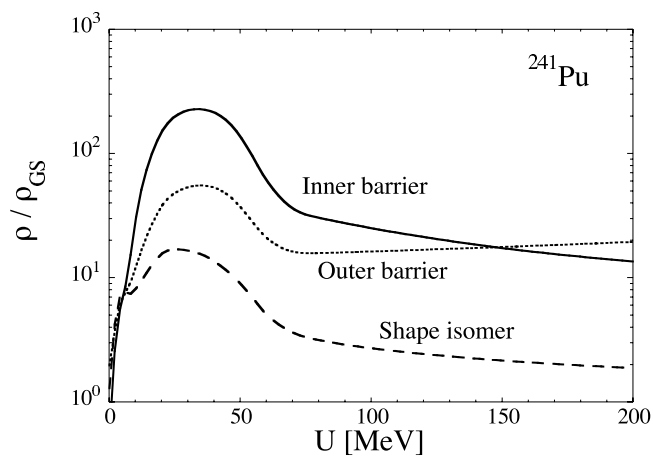


FIG. 3. Total NLD, relative to the GS value, at the inner barrier (solid line), outer barrier (dotted line), or shape isomer (dashed line) as a function of the excitation energy for ^{241}Pu .

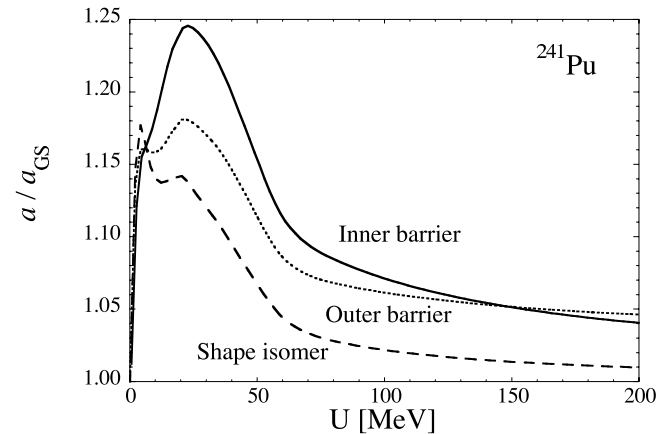


FIG. 4. Plots of the a parameter, relative to the GS value, at the inner barrier (solid line), outer barrier (dotted line), or shape isomer (dashed line) as a function of the excitation energy for ^{241}Pu .

extensive reviews). Such partial level densities can trivially be obtained from our combinatorial approach. Whereas total level densities correspond to the sum of all the partial densities having the same number of particles and holes, state densities with different numbers of particles and holes need to be estimated for applications in pre-equilibrium models. For this reason, all these different ph configurations and the corresponding partial state densities have been computed within the same HFB plus combinatorial method. A detailed analysis, including a comparison with phenomenological models and applications to cross section calculations, is however left for a forthcoming paper.

B. The HFB ingredients for the NLD model

To estimate the NLD, basic nuclear structure properties need to be estimated. These concern the single-particle level scheme ε_i^k including the pairing strength Δ_i^k of each level and the quadrupole deformation parameter β_2 . All these

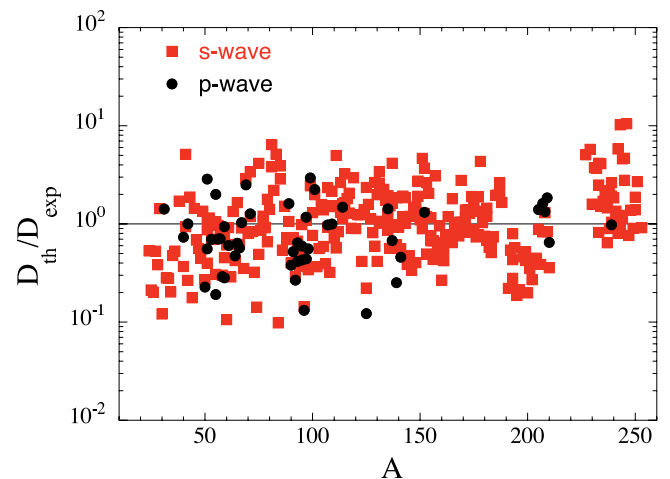


FIG. 5. (Color online) Ratio of HFB plus combinatorial (D_{th}) to the experimental (D_{exp}) s -wave (squares) and p -wave (circles) neutron resonance spacings compiled in Ref. [40].

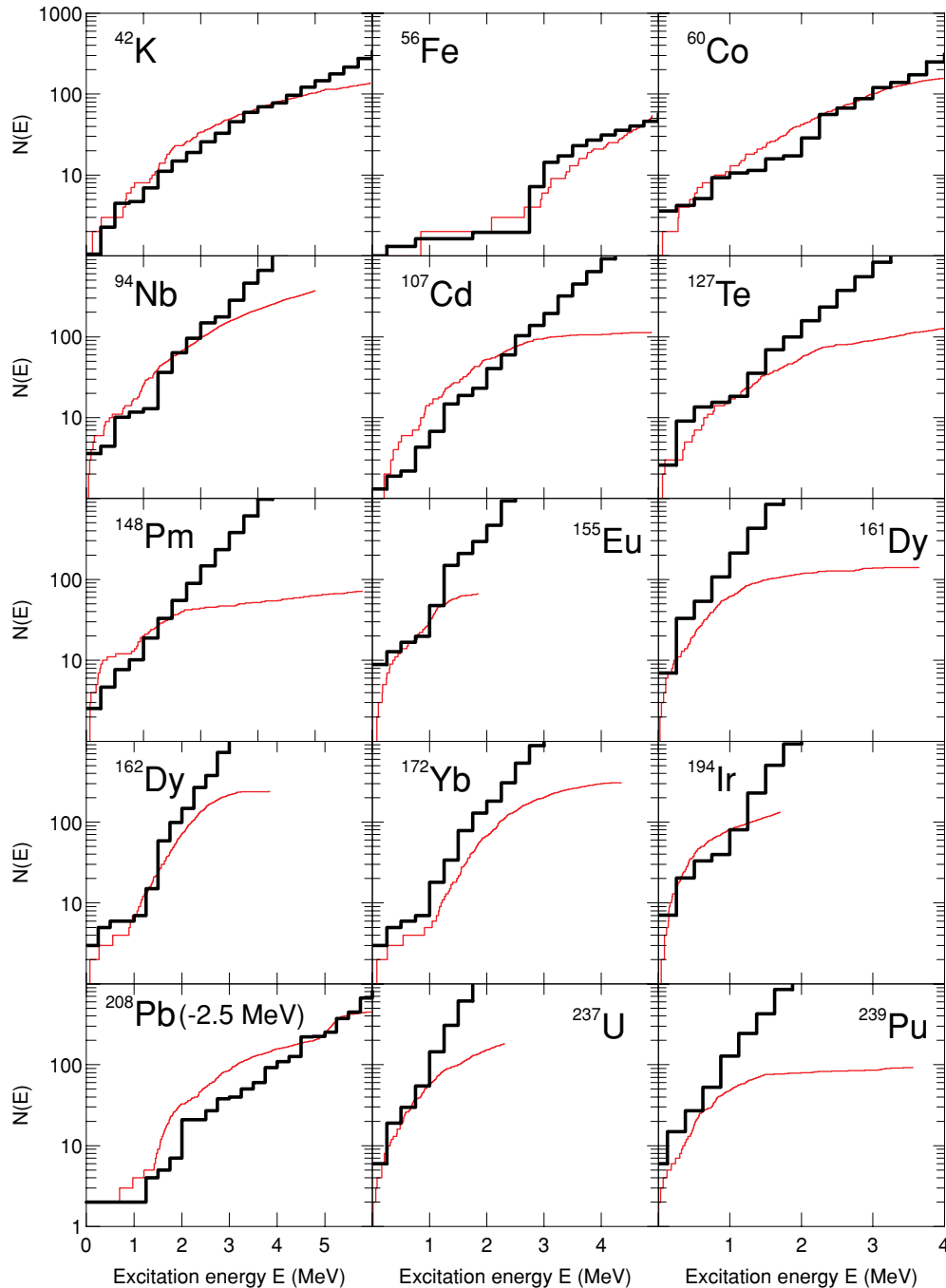


FIG. 6. (Color online) Comparison of the cumulative number of observed levels (thin staircase) with the HFB plus combinatorial predictions (thick line) as a function of the excitation energy U for a sample of 15 nuclei. For ^{208}Pb , both curves have been shifted by 2.5 MeV, so that the energy range corresponds consequently to [2.5–8.5] MeV instead of [0–6] MeV.

quantities have been derived consistently from the recent HFB calculation [38] based on the BSk14 effective interaction. Like the BSk13 force we used in our previous calculation, BSk14 is characterized by a pairing interaction that has been tuned, not only on nuclear binding energy but also in such a way that the spectral gaps $\langle uv\Delta \rangle$ reproduce at best the experimental odd-even mass differences. This condition is of primary importance for a reliable prediction of NLD, as discussed in Ref. [14]. The rms deviation of the HFB-14 mass

model with respect to the 2149 measured masses [39] of nuclei with $Z, N \geq 8$ is 0.729 MeV.

When the excitation energy increases, deformed nuclei tend to become spherical. This shape transition was described in Refs. [13,14] by introducing a phenomenological damping function between the spherical and deformed expressions of the level densities. Such a damping function includes two terms, the first one describing the energy-dependent damping as such and the second one smoothing the NLD between

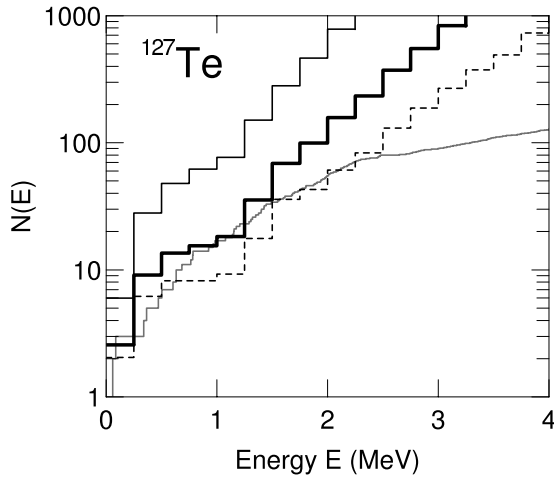


FIG. 7. Cumulative number of levels for ^{127}Te illustrating the impact of the damping function [Eq. (6)]. The gray line shows the experimental levels. The solid thick line results from the mixing of the spherical (dashed line) and deformed (solid thin line) contributions.

deformed and spherical nuclei in the case of slightly deformed nuclei. There is little theoretical or experimental information on the energy at which the shape modification takes place. For this reason, in the present approach this part of the damping function is omitted and only a transitional deformation part for slightly deformed nuclei is retained. The damping function adopted here is given by

$$f_{\text{damp}}(U) = \frac{1}{1 + e^{(E_{\text{def}} - E_{\text{def}}^*)/e}}, \quad (6)$$

where the deformation energy $E_{\text{def}} = E_{\text{sph}} - E_{\text{eq}}$ (coherently estimated from the HFB-14 mass table [38]) is the difference between the energy in the spherical configuration and at the equilibrium deformation, and $E_{\text{def}}^* = 4.5$ MeV defines the transitional deformation energy between spherical and

deformed shapes (with $e = 1.5$ MeV defining the slope of such a transition). Including the weighting function [Eq. (6)] has the advantage of providing a smooth transition from deformed to spherical shapes and consequently reducing part of the uncertainties affecting nuclear structure predictions.

C. NLD at the fission saddle points

Most of the fission calculations make use of the Hill-Wheeler model to estimate the transmission coefficient through the barrier and consequently requires the estimate of the energy-, spin-, and parity-dependent NLD at the fission saddle points and possibly in the isomeric well if absorption in the well and reflection against the second barrier are included in the formalism. The combinatorial approach just described can be applied to the calculation of the NLD at the fission saddle points and isomeric well.

In particular, it should be emphasized that the BSk14 Skyrme force adopted here has also been applied successfully to the calculation of the fission barrier heights. The rms deviation for all 77 primary barriers listed in the RIPL-2 compilation [40] is 1.31 MeV, and it is only 0.67 MeV for the 52 primary barriers of nuclei lower than 9 MeV, the ones of greater astrophysical interest. A similar accuracy is obtained (0.65 MeV) for the 45 secondary experimental barriers necessary for a reliable calculation of fission probabilities. Based on the BSk14 force, the full three-dimensional fission paths have been estimated [38,41] and all the nuclear properties (in particular the single-particle level scheme and pairing properties) have been determined at the saddle points and shape isomer deformations. Based on such inputs, the corresponding NLD have been estimated, coherently within the same framework as the one just detailed for the ground state. The only additional complexity comes from the type of symmetry characterizing the saddle point and isomer shapes [42,43].

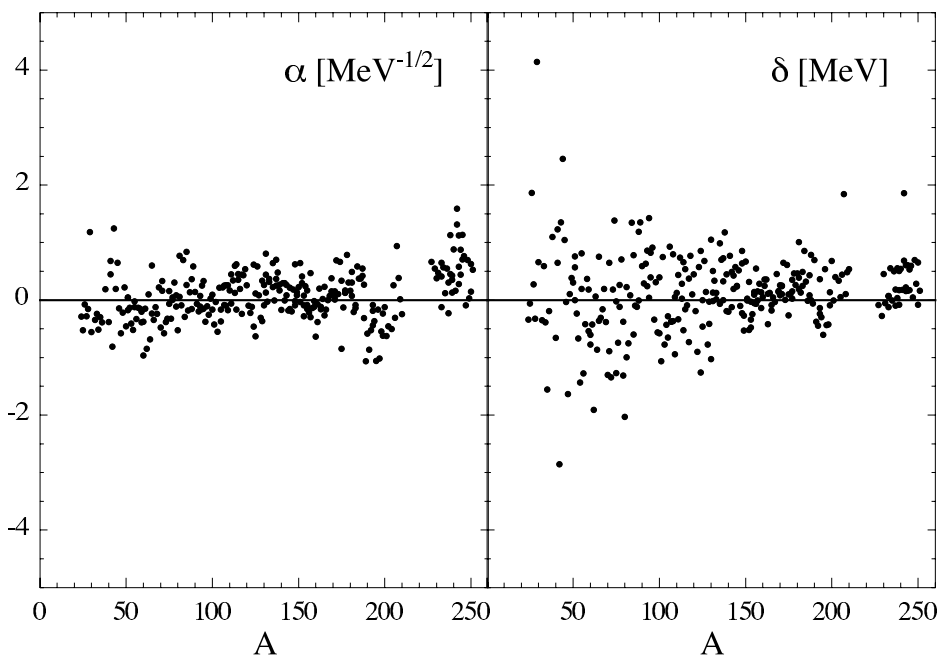


FIG. 8. α and δ values plotted as a function of the atomic mass. See text for more details.

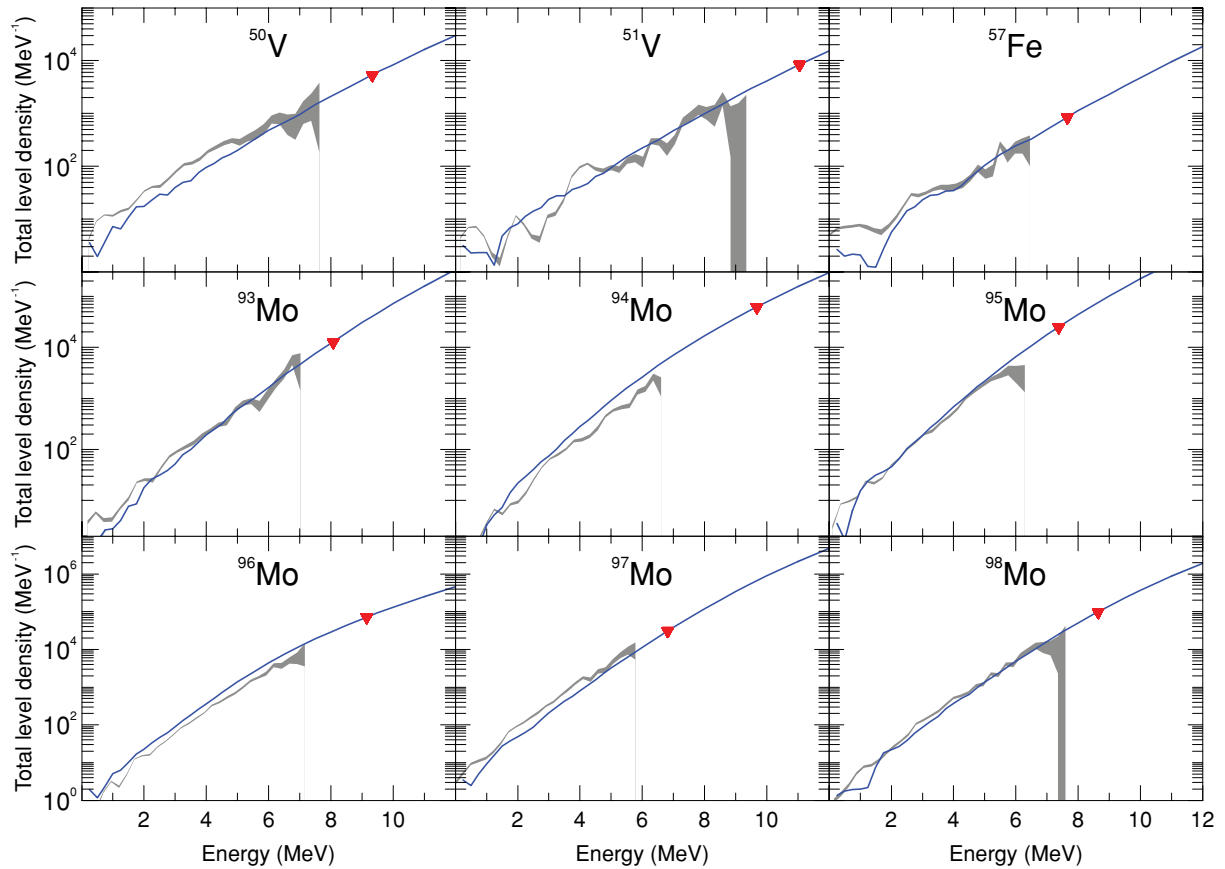


FIG. 9. (Color online) Comparison between the total NLD determined by the Oslo group (gray areas) [49,51] and the HFB combinatorial predictions (solid lines). The full triangles correspond to the model-dependent normalization point derived from the D_0 value at $U = S_n$ [Eq. (1)] by the Oslo group. See text for more details.

The HFB-14 model includes the left-right asymmetry degree of freedom and predicts the outer barrier of actinides to be systematically left-right asymmetric. In this specific case, parity is known not to be a good quantum number. For this reason, the intrinsic NLD calculation is performed without taking an explicit account of parity. The equipartition of both parities is then assumed. Triaxial degree of freedom is not included in the HFB-14 model, although the inner barriers of actinides is known to be in general triaxial (and left-right symmetric) [44,45]. In this case, the fission level density still needs to be multiplied by the enhancement factor $K_{\text{sym}} = \sqrt{\pi/2}\sigma_{\perp}$ [42,43], where σ_{\perp} is the spin cutoff factor perpendicular to the symmetry axis. This factor is however not included in the present calculation since HFB-14 inner barriers are always axially symmetric. It should be remembered that no microscopic calculations including triaxiality and left-right asymmetry have ever been performed.

As an illustration, we compare in Fig. 3 the total NLD at the ground state (GS) with the one at the inner and outer barriers as well as the shape isomer of ^{241}Pu . The inner barrier and isomer deformations are taken as axially symmetric, whereas the outer barrier deformation is left-right asymmetric. The deformation and barrier height predicted by the HFB-14 model are, respectively, $\beta_2 = 0.51$, $B_f = 6.5$ MeV for the inner barrier and $\beta_2 = 1.3$, $B_f = 5.8$ MeV for the outer barrier

and for the isomer $\beta_2 = 0.9$ and $E_m = 1.8$ MeV. The NLD is seen to be the largest for the inner barrier, although it is located at a smaller deformation. Above some 40 MeV, shell effects have disappeared, leaving an almost U -independent ratio representative of the pairing shift.

Since the NLD at the fission saddle point is often expressed in terms of the level density parameter a_f relative to the GS value, we estimated the corresponding a_f/a_{GS} ratio assuming the a parameter can be determined from the approximate Fermi-gas relation

$$\rho(U) = \frac{\sqrt{\pi}}{12a^{1/4}U^{5/4}} \exp(2\sqrt{aU}), \quad (7)$$

where $\rho(U)$ corresponds to the total NLD obtained in the present work, either at the GS or at the fission saddle point or isomeric deformation. Note that in Eq. (7) it is assumed that both the shell and pairing effects but also the rotational enhancement factor are implicitly included in the a parameter. We illustrate in Fig. 4 the corresponding ratios in the specific case of ^{241}Pu . Some complex structures including all shell, pairing, and deformation effects are observed below 20 MeV.

The final NLD at the ground state and fission saddle points have been tested in the calculation of neutron-induced fission cross section [15,46]. It is shown that a very satisfactory agreement with experimental cross sections can be achieved.

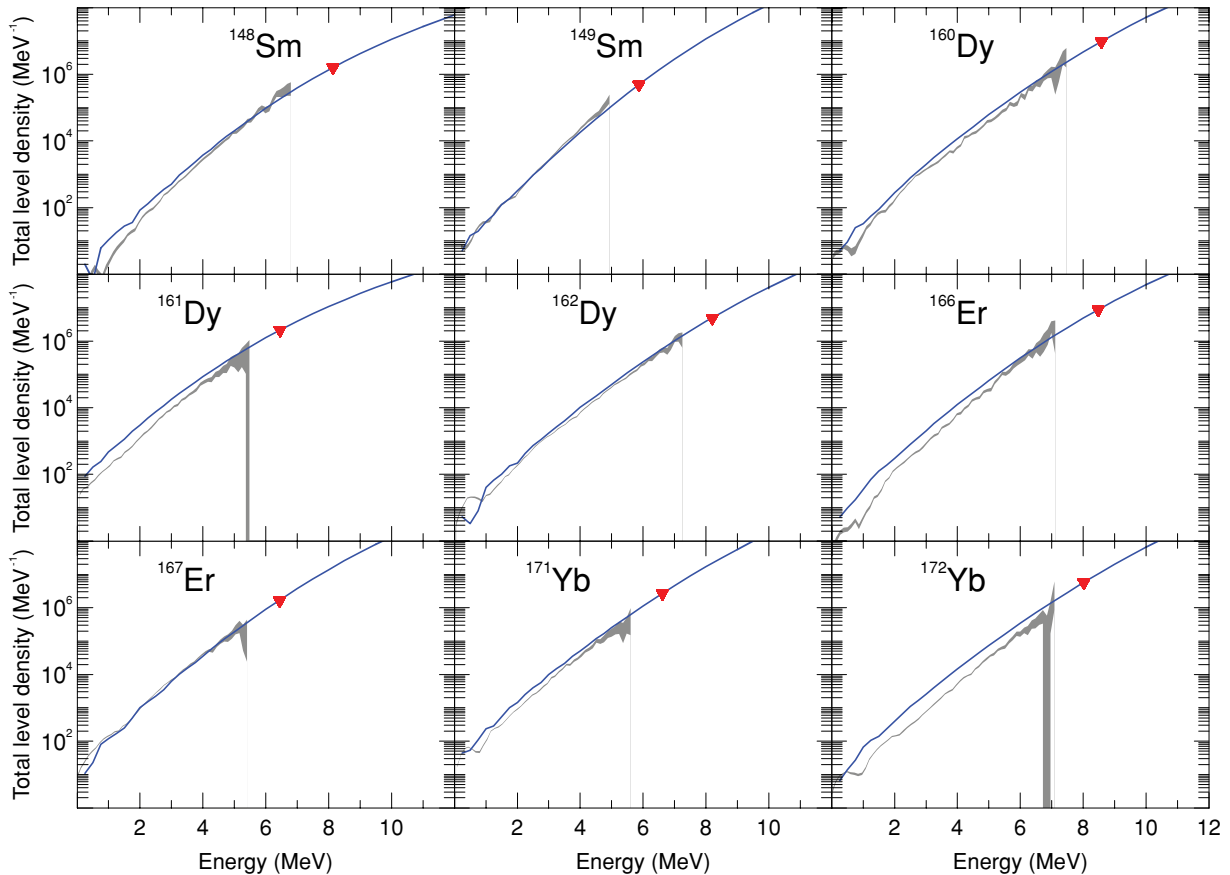


FIG. 10. (Color online) Same as Fig. 9 but for other isotopes.

III. COMPARISON WITH EXPERIMENTAL DATA

The new NLD are now compared with experimental data. In spite of considerable experimental efforts made to derive NLD, the lack of reliable data—especially over a wide energy range—constitutes the main problem that the NLD theories have to face. Nevertheless, numerous analyses of slow neutron resonances and of cumulative numbers of low-energy levels have greatly helped to provide experimental information on NLD. Other sources of information have also been suggested, such as analyses of spectra of evaporated particles and coherence widths of cross section fluctuations. However, most of these experimental data are affected by systematic errors resulting from experimental uncertainties as well as the use of approximate theories to analyze them.

The most extensive and reliable source of experimental information on NLD remains the *s*- and *p*-wave neutron resonance spacings [5,40] and the observed low-energy excited levels [40]. Note, however, that different compilations of resonance spacings show non-negligible differences, especially for spherical nuclei, for which only a few neutron resonances are observed. We show in Fig. 5 the result of our HFB plus combinatorial approach with respect to experimental *s*- and *p*-wave spacings compiled in the RIPL-2 database [40].

The quality of a global NLD formula can be described by the rms deviation factor defined as

$$f_{\text{rms}} = \exp \left[\frac{1}{N_e} \sum_{i=1}^{N_e} \ln^2 \frac{D_{\text{th}}^i}{D_{\text{exp}}^i} \right]^{1/2}, \quad (8)$$

where $D_{\text{th}}(D_{\text{exp}})$ is the theoretical (experimental) resonance spacing and N_e is the number of nuclei in the compilation. Globally, the D values are predicted within a factor of 2 (with the exact rms factor amounting to $f_{\text{rms}} = 2.3$ for both the *s*- and *p*-wave data). This result is to be compared to the $f_{\text{rms}} = 1.80$ deviation of the global back-shifted Fermi gas (BSFG) formula [2] and the $f_{\text{rms}} = 2.14$ value obtained with our previous combinatorial result. Our new approach therefore gives rather comparable predictions with respect to the other existing global models.

The HFB plus combinatorial model also gives satisfactory extrapolations to low energies. As an example, we compare in Fig. 6 the predicted cumulative number of levels $N(U)$ with the experimental data [40] for the same 15 nuclei as the one presented in Ref. [14], including light as well as heavy, spherical, and deformed species. Globally, the present model provides results similar to those illustrated in Ref. [14]. The case of ^{127}Te is worth discussing, since the description is now much better than it used to be. This stems from the new

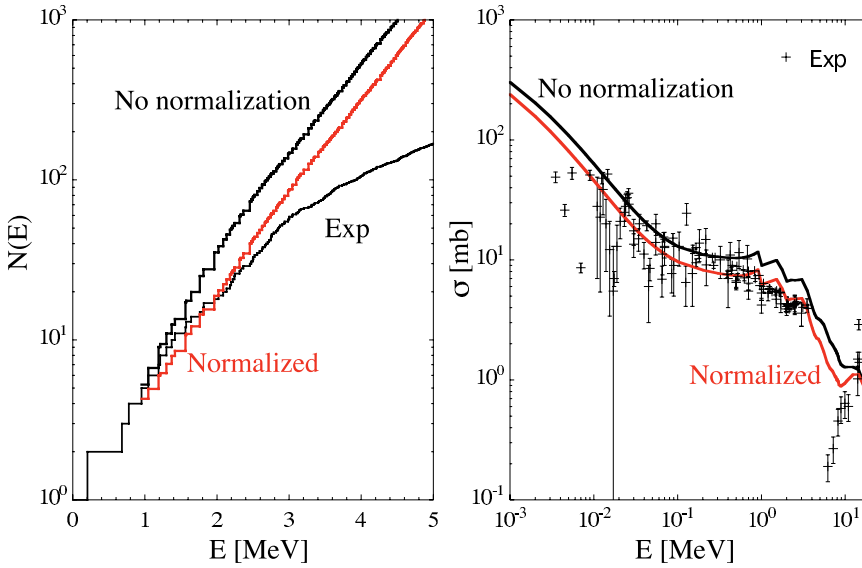


FIG. 11. (Color online) (Left) Cumulative number of levels predicted by our NLD for ^{90}Y with and without normalization (see Table I for the corresponding α and δ parameters). The experimental curve is shown for comparison. (Right) $^{89}\text{Y}(n, \gamma)^{90}\text{Y}$ cross section obtained using the raw and normalized NLD and compared with experimental data [58].

damping function given by Eq. (6) (see Sec. II B). As can be observed in Fig. 7, whereas in Ref. [14], ^{127}Te was rather considered as a deformed nucleus at low energy (full thin line), it is now described by a mixing between the spherical (dashed line) and deformed configurations. The mixing given by Eq. (6) yields the full thick curve, which is in better agreement with experimental data. However, we still find situations where the spherical/deformed character of the nucleus is not satisfactory.

For many nuclear physics applications a renormalization procedure of the NLD on experimental data is required, in particular for nuclear data evaluation or for an accurate and reliable estimate of reaction cross sections. Though the HFB plus combinatorial NLD are provided in a table format, it is possible to renormalize them on both the experimental level scheme at low energy and the neutron resonance spacings at $U = S_n$ in a way similar to what is usually done with analytical formulas. More specifically, the renormalized level density can be corrected through the expression

$$\rho(U, J, P)_{\text{renorm}} = e^{\alpha\sqrt{U-\delta}} \times \rho(U - \delta, J, P), \quad (9)$$

where the energy shift δ is essentially extracted from the analysis of the cumulative number of levels and α from the experimental s -wave neutron spacing. With such a renormalization, the experimental low-lying states and the D_{exp} values can be reproduced reasonably well, as discussed in detail in Ref. [2]. Equation (9) has been used to fit the 289 nuclides for which both an experimental s -wave spacing (D_0) and a discrete level sequence exist. The corresponding δ and α values for these nuclei are given in Table I and shown graphically in Fig. 8. Interestingly, the α and δ parameters show no systematic trend or A dependence and more particularly no correlation with shell closures. For an additional 846 nuclides, only the experimental discrete level scheme with at least 10 levels is known. For those nuclei, only the δ shift is used to reproduce at best the low-lying levels.

Finally, we have compared our NLD calculations with the experimental data extracted by the Oslo group from the analy-

sis of particle- γ coincidence in the ($^3\text{He}, \alpha\gamma$) and ($^3\text{He}, ^3\text{He}'\gamma$) reactions [47–55]. The total NLD $\rho_{\text{tot}}(U) = \sum_{J,\pi} \rho(U, J, \pi)$ are compared with our microscopic results in Figs. 9 and 10 for several isotopes. It should be stressed that such an experimental determination is however model-dependent. To extract the absolute value of the total level density from the measured data, the so-called experimental NLD needs to be normalized by the total level density at the neutron binding energy, which in turn is derived from the neutron resonance spacing. In practice, to deduce the total level density from the D_0 value, both the spin and parity distributions at $U = S_n$ are required. If the equipartition of the parity distribution is relatively well established at these energies, discrepancies can stand from the adopted spin distribution. In particular, it is clear that a nonstatistical approach such as the combinatorial method might provide different spin distributions than the simple shell- and pairing-independent Gaussian spin distribution assumed within the BSFG model [56] (and adopted by the Oslo group).

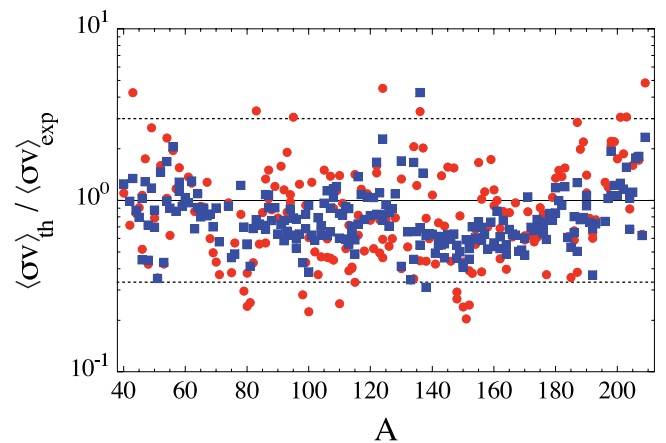


FIG. 12. (Color online) Ratio of TALYS Maxwellian-averaged (n, γ) rates $(\sigma v)_{\text{th}}$ with experimental values [59] at $T = 3 \times 10^8$ K obtained by using the raw NLD (circles) and those normalized (squares) according to the method described in Sec. III.

TABLE I. Values of the δ and α parameters [see Eq. (9)] for the 289 nuclei for which both an experimental D_0 value and a discrete level sequence are known.

Nucleus	α	δ	Nucleus	α	δ	Nucleus	α	δ
²⁴ Na	-0.28	-0.34	⁷¹ Zn	0.33	0.65	¹⁰⁸ Pd	-0.09	0.80
²⁵ Mg	-0.52	-0.06	⁷⁰ Ga	-0.48	-1.30	¹⁰⁹ Pd	-0.17	-0.94
²⁶ Mg	-0.07	1.87	⁷² Ga	-0.58	-1.34	¹¹¹ Pd	0.45	-0.33
²⁷ Mg	-0.28	0.28	⁷¹ Ge	0.17	-0.89	¹⁰⁸ Ag	0.26	-0.37
²⁸ Al	-0.15	-0.32	⁷³ Ge	-0.38	0.18	¹¹⁰ Ag	0.17	0.12
²⁹ Si	1.19	4.14	⁷⁴ Ge	-0.32	1.38	¹⁰⁷ Cd	0.25	-0.37
³⁰ Si	-0.56	0.66	⁷⁵ Ge	-0.06	-0.03	¹⁰⁹ Cd	0.26	0.05
³² P	-0.34	-0.35	⁷⁷ Ge	0.00	-0.12	¹¹¹ Cd	-0.06	0.44
³³ S	-0.24	0.59	⁷⁶ As	-0.32	-0.74	¹¹² Cd	0.34	0.74
³⁴ S	-0.51	-0.39	⁷⁵ Se	0.16	-1.27	¹¹³ Cd	0.13	0.02
³⁵ S	-0.29	-1.55	⁷⁷ Se	0.04	0.26	¹¹⁴ Cd	0.62	0.66
³⁶ Cl	-0.39	-0.19	⁷⁸ Se	0.31	0.71	¹¹⁵ Cd	0.35	-0.16
³⁸ Cl	0.19	1.10	⁷⁹ Se	-0.11	-1.31	¹¹⁷ Cd	-0.24	-0.73
⁴¹ Ar	0.68	1.23	⁸¹ Se	0.77	0.23	¹¹⁴ In	-0.16	-0.52
⁴⁰ K	-0.38	-0.66	⁸³ Se	0.70	0.08	¹¹⁶ In	0.19	-0.09
⁴² K	-0.81	-2.86	⁸⁰ Br	-0.53	-2.03	¹¹³ Sn	0.60	0.28
⁴¹ Ca	0.45	0.65	⁸² Br	-0.09	-0.75	¹¹⁵ Sn	0.45	0.54
⁴³ Ca	1.25	1.35	⁷⁹ Kr	0.08	-0.38	¹¹⁷ Sn	0.44	0.38
⁴⁴ Ca	0.19	2.46	⁸¹ Kr	0.06	-1.00	¹¹⁸ Sn	0.43	0.77
⁴⁵ Ca	0.65	1.05	⁸⁴ Kr	-0.29	1.35	¹¹⁹ Sn	0.54	0.10
⁴⁶ Sc	-0.14	-0.03	⁸⁵ Kr	0.84	0.78	¹²⁰ Sn	0.26	0.45
⁴⁷ Ti	-0.58	-1.63	⁸⁶ Rb	-0.18	-0.10	¹²¹ Sn	-0.10	-0.19
⁴⁸ Ti	-0.22	0.11	⁸⁸ Rb	-0.15	0.00	¹²⁵ Sn	-0.63	0.00
⁴⁹ Ti	0.22	0.38	⁸⁵ Sr	0.26	-0.60	¹²² Sb	-0.22	-0.90
⁵⁰ Ti	-0.46	0.31	⁸⁷ Sr	0.13	-0.12	¹²⁴ Sb	-0.46	-1.26
⁵¹ Ti	0.05	0.00	⁸⁸ Sr	0.36	1.19	¹²³ Te	-0.12	0.58
⁵¹ V	-0.18	0.76	⁸⁹ Sr	0.58	1.35	¹²⁴ Te	0.62	0.86
⁵² V	-0.13	-0.23	⁹⁰ Y	0.14	0.59	¹²⁵ Te	0.12	-0.46
⁵¹ Cr	0.04	0.57	⁹¹ Zr	-0.06	0.29	¹²⁶ Te	0.59	0.68
⁵³ Cr	-0.41	-0.66	⁹² Zr	-0.20	0.63	¹²⁷ Te	0.08	0.14
⁵⁴ Cr	-0.52	-1.43	⁹³ Zr	0.07	0.86	¹²⁹ Te	0.34	-0.03
⁵⁵ Cr	-0.02	0.19	⁹⁴ Zr	0.25	1.43	¹³¹ Te	0.81	0.51
⁵⁶ Mn	-0.33	-1.27	⁹⁵ Zr	0.33	0.82	¹²⁸ I	-0.31	-0.77
⁵⁵ Fe	-0.13	0.81	⁹⁴ Nb	-0.16	0.04	¹³⁰ I	-0.09	-1.02
⁵⁷ Fe	-0.13	-0.42	⁹³ Mo	-0.11	0.24	¹²⁹ Xe	-0.37	-0.41
⁵⁸ Fe	-0.15	0.37	⁹⁵ Mo	-0.15	0.40	¹³⁰ Xe	0.26	1.05
⁵⁹ Fe	-0.39	-0.54	⁹⁶ Mo	-0.37	0.91	¹³¹ Xe	0.44	-0.02
⁶⁰ Co	-0.38	-0.60	⁹⁷ Mo	-0.11	-0.34	¹³² Xe	-0.03	0.34
⁵⁹ Ni	-0.20	0.18	⁹⁸ Mo	-0.25	0.31	¹³³ Xe	0.37	0.13
⁶⁰ Ni	-0.96	-0.78	⁹⁹ Mo	0.02	-0.56	¹³⁵ Xe	0.64	0.99
⁶¹ Ni	-0.15	-0.43	¹⁰¹ Mo	-0.42	-1.07	¹³⁷ Xe	0.25	0.00
⁶² Ni	-0.84	-1.91	¹⁰⁰ Tc	-0.16	-0.58	¹³⁴ Cs	-0.35	-1.30
⁶³ Ni	0.10	0.06	¹⁰⁰ Ru	0.09	0.40	¹³¹ Ba	0.13	0.13
⁶⁵ Ni	0.60	0.76	¹⁰² Ru	-0.03	0.75	¹³³ Ba	0.32	0.01
⁶⁴ Cu	-0.68	-0.86	¹⁰³ Ru	-0.55	-0.77	¹³⁵ Ba	0.23	-0.06
⁶⁶ Cu	-0.34	-0.31	¹⁰⁵ Ru	-0.37	-0.28	¹³⁶ Ba	-0.01	0.70
⁶⁵ Zn	-0.23	-0.36	¹⁰⁴ Rh	0.22	-0.43	¹³⁷ Ba	0.37	0.73
⁶⁷ Zn	-0.12	-0.16	¹⁰⁵ Pd	-0.17	-0.65	¹³⁸ Ba	0.48	1.18
⁶⁸ Zn	-0.24	0.19	¹⁰⁶ Pd	0.22	0.93	¹³⁹ Ba	0.27	0.45
⁶⁹ Zn	0.22	-0.38	¹⁰⁷ Pd	-0.09	-0.37	¹³⁹ La	0.17	-0.19
¹⁴⁰ La	-0.17	-0.20	¹⁶⁷ Er	0.00	-0.03	¹⁹⁸ Au	-0.55	-0.42
¹³⁷ Ce	0.70	0.32	¹⁶⁸ Er	0.07	0.45	¹⁹⁹ Hg	-0.23	-0.09
¹⁴¹ Ce	0.30	0.77	¹⁶⁹ Er	0.15	0.14	²⁰⁰ Hg	-0.12	0.68
¹⁴² Ce	0.30	0.49	¹⁷¹ Er	0.15	0.11	²⁰¹ Hg	-0.62	0.00
¹⁴³ Ce	0.08	0.19	¹⁷⁰ Tm	0.10	0.08	²⁰² Hg	-0.45	0.40
¹⁴² Pr	-0.01	-0.12	¹⁷¹ Tm	0.07	0.25	²⁰⁴ Tl	-0.50	0.34

TABLE I. (*Continued.*)

Nucleus	α	δ	Nucleus	α	δ	Nucleus	α	δ
¹⁴³ Nd	0.26	0.43	¹⁶⁹ Yb	0.38	0.16	²⁰⁶ Tl	-0.31	0.44
¹⁴⁴ Nd	-0.18	0.57	¹⁷⁰ Yb	0.14	0.26	²⁰⁵ Pb	0.26	0.05
¹⁴⁵ Nd	0.21	0.24	¹⁷¹ Yb	0.01	0.24	²⁰⁷ Pb	0.94	1.84
¹⁴⁶ Nd	-0.19	0.52	¹⁷² Yb	0.69	0.65	²⁰⁸ Pb	0.38	0.11
¹⁴⁷ Nd	0.18	-0.10	¹⁷³ Yb	0.11	0.01	²⁰⁹ Pb	0.02	0.48
¹⁴⁸ Nd	0.62	0.85	¹⁷⁴ Yb	0.66	0.61	²¹⁰ Bi	-0.24	0.54
¹⁴⁹ Nd	0.08	-0.53	¹⁷⁵ Yb	0.34	0.10	²²⁷ Ra	0.67	-0.08
¹⁵¹ Nd	0.65	0.02	¹⁷⁷ Yb	0.17	0.15	²²⁹ Th	0.55	-0.27
¹⁴⁸ Pm	-0.02	-0.22	¹⁷⁶ Lu	-0.13	0.11	²³⁰ Th	0.38	0.46
¹⁴⁵ Sm	-0.15	0.25	¹⁷⁷ Lu	0.12	0.35	²³¹ Th	0.47	-0.05
¹⁴⁸ Sm	-0.09	0.64	¹⁷⁵ Hf	-0.85	-0.26	²³³ Th	0.65	0.07
¹⁴⁹ Sm	0.14	-0.27	¹⁷⁷ Hf	0.13	0.03	²³³ Pa	-0.12	-0.13
¹⁵⁰ Sm	0.23	0.67	¹⁷⁸ Hf	0.78	0.46	²³³ U	0.41	0.07
¹⁵¹ Sm	-0.03	0.00	¹⁷⁹ Hf	0.30	0.26	²³⁴ U	0.57	0.55
¹⁵² Sm	0.41	0.31	¹⁸⁰ Hf	0.17	0.46	²³⁵ U	0.12	-0.01
¹⁵³ Sm	-0.09	-0.34	¹⁸¹ Hf	0.49	0.39	²³⁶ U	0.55	0.50
¹⁵⁵ Sm	0.17	0.10	¹⁸¹ Ta	0.30	1.01	²³⁷ U	0.30	0.18
¹⁵² Eu	0.29	-0.52	¹⁸² Ta	-0.21	0.13	²³⁸ U	1.13	0.56
¹⁵³ Eu	-0.28	-0.03	¹⁸³ Ta	-0.14	0.49	²³⁹ U	0.36	0.51
¹⁵⁴ Eu	0.24	-0.24	¹⁸¹ W	0.07	0.19	²³⁷ Np	-0.23	-0.10
¹⁵⁵ Eu	-0.09	0.14	¹⁸³ W	-0.09	0.25	²³⁸ Np	0.45	0.04
¹⁵⁶ Eu	-0.22	-0.06	¹⁸⁴ W	0.59	0.86	²³⁹ Np	0.13	-0.08
¹⁵³ Gd	0.08	-0.48	¹⁸⁵ W	0.37	0.32	²³⁹ Pu	0.43	0.17
¹⁵⁵ Gd	-0.15	-0.05	¹⁸⁷ W	0.55	0.43	²⁴⁰ Pu	0.88	0.54
¹⁵⁶ Gd	-0.15	0.55	¹⁸⁶ Re	0.37	-0.01	²⁴¹ Pu	0.17	0.18
¹⁵⁷ Gd	-0.30	0.15	¹⁸⁸ Re	0.27	0.00	²⁴² Pu	1.32	0.69
¹⁵⁸ Gd	-0.14	0.29	¹⁸⁷ Os	0.42	0.08	²⁴³ Pu	1.13	0.22
¹⁵⁹ Gd	-0.12	0.13	¹⁸⁸ Os	-0.32	0.78	²⁴⁵ Pu	1.14	0.53
¹⁶¹ Gd	-0.07	0.36	¹⁸⁹ Os	-1.06	-0.06	²⁴² Am	1.59	1.86
¹⁶⁰ Tb	-0.64	0.05	¹⁹⁰ Os	-0.58	0.70	²⁴³ Am	0.58	0.16
¹⁵⁷ Dy	0.47	-0.01	¹⁹¹ Os	-0.86	-0.38	²⁴⁴ Am	0.88	0.16
¹⁵⁹ Dy	-0.02	-0.14	¹⁹³ Os	-0.09	0.36	²⁴³ Cm	0.28	0.61
¹⁶¹ Dy	-0.38	0.25	¹⁹² Ir	-0.52	-0.45	²⁴⁴ Cm	0.44	0.61
¹⁶² Dy	0.20	0.36	¹⁹³ Ir	-0.44	-0.14	²⁴⁵ Cm	0.71	0.18
¹⁶³ Dy	-0.16	-0.42	¹⁹⁴ Ir	-0.37	-0.29	²⁴⁶ Cm	0.76	0.60
¹⁶⁴ Dy	0.02	0.12	¹⁹³ Pt	-0.19	-0.24	²⁴⁷ Cm	-0.09	0.05
¹⁶⁵ Dy	0.23	-0.09	¹⁹⁵ Pt	-1.06	-0.60	²⁴⁸ Cm	0.70	0.70
¹⁶⁶ Ho	-0.16	0.05	¹⁹⁶ Pt	-0.16	0.54	²⁴⁹ Cm	0.03	0.29
¹⁶³ Er	-0.11	0.11	¹⁹⁷ Pt	-1.02	-0.43	²⁵⁰ Bk	0.15	-0.08
¹⁶⁵ Er	-0.26	-0.18	¹⁹⁹ Pt	-0.62	0.14	²⁵⁰ Cf	0.63	0.65

For a meaningful comparison between our predictions and the Oslo data, it is therefore important to normalize our level densities to the level density value at $U = S_n$ considered by the Oslo group. This is done by renormalizing our predictions by Eq. (9) for each isotope, with an α parameter given by

$$\rho_{\text{HFB}}(S_n) \times \exp(\alpha\sqrt{S_n}) = \rho_{\text{Oslo}}(S_n). \quad (10)$$

As can be observed, with such a normalization, the combinatorial NLD agree extremely well with the so-called experimental NLD below S_n .

In Table II, the total level densities at $U = S_n$ estimated by the Oslo group are compared with the value we derived from our NLD model on the basis of the same s -wave spacing (whenever available) as the one used by the Oslo

group. Note that the Oslo group determined the density on the basis of a BSFG model, by assuming in particular a parity equipartition for all spin distributions but also a shell- and pairing-independent spin cutoff factor. None of these approximations are made in our approach. When no D_0 value is available the total NLD corresponds to our prediction that can be compared to the value deduced from systematics by the Oslo group. Note again that the total level density at S_n is fundamental to determining absolute level densities from the Oslo method. As seen in Table II, differences between the Oslo and HFB level densities can reach a factor up to 3.7 for ¹⁷²Yb or down to 0.5 for ⁵¹V. In most cases, our NLD model predicts larger values. Although the BSFG model provides a relatively uncertain prescription to derive the total level density from the D_0 value, the values determined by

TABLE II. Experimental D_0 and corresponding total density ρ_{Oslo} at $U = S_n$ used by the Oslo group for the 18 nuclei shown in Figs. 9 and 10. When no reference to the D_0 value is found in the papers of the Oslo group, the value tabulated in the RIPL-2 database [40] is adopted. The density ρ_{HFB} corresponds to the total level density deduced from the same D_0 value using the present HFB plus combinatorial model renormalized by the α and δ parameters [see Eq. (9)]; the cumulative number of low-lying state is also reproduced in this procedure].

Nucleus	S_n (MeV)	D_0 (eV)	ρ_{Oslo} (MeV^{-1})	ρ_{HFB} (MeV^{-1})	$\rho_{\text{HFB}}/\rho_{\text{Oslo}}$
^{50}V	9.330	–	5.40×10^3	8.59×10^3	1.59
^{51}V	11.050	2300 ^a	8.4×10^3	4.07×10^3	0.48
^{57}Fe	7.646	25400 ^b	8.53×10^2	1.74×10^3	2.04
^{93}Mo	8.067	2700 ^a	1.27×10^4	2.21×10^4	1.74
^{94}Mo	9.678	–	6.20×10^4	1.57×10^5	2.53
^{95}Mo	7.367	1320 ^a	2.50×10^4	5.03×10^4	2.01
^{96}Mo	9.154	105 ^a	7.18×10^4	1.35×10^5	1.88
^{97}Mo	6.821	1050 ^a	3.20×10^4	5.44×10^4	1.75
^{98}Mo	8.642	75 ^a	9.99×10^4	1.53×10^5	1.54
^{148}Sm	8.140	5.7 ^a	1.59×10^6	1.82×10^6	1.15
^{149}Sm	5.870	100 ^a	4.90×10^5	7.96×10^5	1.63
^{160}Dy	8.576	–	9.70×10^6	1.27×10^7	1.31
^{161}Dy	6.454	27 ^a	2.14×10^6	4.98×10^6	2.33
^{162}Dy	8.197	2.4 ^a	4.96×10^6	1.00×10^7	2.02
^{166}Er	8.474	–	8.67×10^6	6.30×10^6	0.73
^{167}Er	6.436	38 ^b	1.68×10^6	2.90×10^6	1.73
^{171}Yb	6.615	33 ^b	2.72×10^6	3.65×10^6	1.34
^{172}Yb	8.020	5.8 ^b	5.81×10^6	2.15×10^7	3.70

^aData taken from the papers of the Oslo group [47–55].

^bData taken from the RIPL-2 compilation [40].

the Oslo group cannot be ruled out. This shows that globally the experimental uncertainties on the Oslo method are more likely underestimated and should be revisited in the light of additional NLD models, like ours, that differ from the BSFG approach.

IV. APPLICATION TO REACTION CROSS SECTION CALCULATIONS

In the present section, the HFB plus combinatorial NLD are used to calculate reaction cross sections within the Hauser-Feshbach formalism. The code TALYS is used for this purpose [57]. As an illustration, we show in Fig. 11, the specific case of the $^{89}\text{Y}(n, \gamma)^{90}\text{Y}$ cross section. The NLD predicted for ^{90}Y is shown in Fig. 11 (left panel) before and after the renormalization procedure. When the renormalization is applied (in this case to all the nuclei involved in the nuclear reaction processes), the cross section is seen to be better described.

To evaluate the overall quality of the NLD, we compare in Fig. 12 the Maxwellian-averaged (n, γ) rates (σv) at $T = 3 \times 10^8$ K with experimental data for some 219 nuclei heavier than ^{40}Ca included in the compilation of Bao *et al.* [59]. The radiative capture rates at such a temperature essentially reflect the cross section around a 25-keV incident neutron energy. At such energies, the radiative capture cross section is known to be very sensitive to the NLD below the neutron threshold. It appears that the calculations agree with experimental data

roughly within a factor of 2. Note that additional uncertainties stemming in particular from γ -ray strength functions also affect the predictions. A strong correlation between the deviations seen in the rates of Fig. 12 and the NLD of Fig. 5 can be observed.

If we now use the NLD renormalized on experimental data (see Sec. III) to estimate the reaction rates, the deviations with respect to experimental rates are clearly less dispersed than with the raw NLD (Fig. 12). The corresponding rms deviation [based on a relation identical to Eq. (8)] for the 219 nuclei is $f_{\text{rms}} = 1.92$ using the raw NLD and 1.60 with the renormalized NLD.

V. CONCLUSIONS

The combinatorial method introduced in Ref. [14] has been updated to improve the description of the collective vibrational levels. This has been performed by using the boson partition function [11]. The resulting NLD are qualitatively similar to those we obtained assuming a phenomenological vibrational enhancement factor [14], both for the cumulative number of discrete levels and the mean s - and p -wave resonance spacings. Our total level densities also agree fairly with the values extracted from the analysis of particle- γ coincidence in the ($^3\text{He}, \alpha\gamma$) and ($^3\text{He}, ^3\text{He}'\gamma$) reactions, at least if normalized on the same density at the neutron binding energy. The combinatorial model has also been applied to estimate the NLD on top of the fission barriers and in the isomeric well. Finally,

within the same framework, particle-hole NLD required for pre-equilibrium reaction models have been determined.

The final NLD (without renormalization on experimental data) are available to the scientific community at the Web site <http://www-astro.ulb.ac.be>. The tables include the spin- and parity-dependent NLD for more than 8500 nuclei ranging from $Z = 8$ to $Z = 110$ for a large energy and spin grid ($U = 0$ to 200 MeV and the lowest 30 spins). No simple analytical fit to the tabulated NLD is given to avoid losing the specific microscopic characteristics of the model. It should be stressed that the combinatorial NLD cannot be approximated by a simple BSFG-type formula, except at very high energies (above roughly 100 MeV), where the shell, pairing, and deformation effects disappear.

The NLD have also been implemented in the TALYS reaction code (publicly available at <http://www.talys.eu>), where the normalization parameters given in Sec. III (Table I) are also included. As we have shown, when experimental cross sections are available our normalization procedure globally improves the agreement with the data.

Still, some improvements may be required. In particular, the spherical/deformed character for transitional nuclei is not yet under control. In addition, at increasing energies, the shape of the nucleus changes, so that building the excitation configurations on top of the ground-state single-particle properties may not be adequate. Such effects will be studied in the near future.

-
- [1] H. A. Bethe, Phys. Rev. **50**, 332 (1936).
 [2] A. J. Koning, S. Hilaire, and S. Goriely, Nucl. Phys. **A810**, 13 (2008).
 [3] S. Goriely, Nucl. Phys. **A605**, 28 (1996).
 [4] A. V. Ignatyuk, IAEA Report INDC(CCP)-233/L, 1985.
 [5] A. V. Ignatyuk, IAEA Report TECDOC-1034, 1998.
 [6] P. Decowski *et al.*, Nucl. Phys. **A110**, 129 (1968).
 [7] L. G. Moretto, Nucl. Phys. **A185**, 145 (1972).
 [8] M. Hillman and J. R. Grover, Phys. Rev. **185**, 1303 (1968).
 [9] S. Hilaire and J. P. Delaroche, in *International Conference on Nuclear Data for Science and Technology: Trieste, 19–24 May 1997*, edited by G. Reffo, A. Ventura, and C. Grandi (Italian Physical Society, Rome, 1997), Vol. 1, p. 694.
 [10] S. Hilaire, J. P. Delaroche, and A. J. Koning, Nucl. Phys. **A632**, 417 (1998).
 [11] S. Hilaire, J. P. Delaroche, and M. Girod, Eur. Phys. J. **A12**, 169 (2001).
 [12] Y. Alhassid, S. Liu, and H. Nakada, Phys. Rev. Lett. **83**, 4265 (1999).
 [13] P. Demetriou and S. Goriely, Nucl. Phys. **A695**, 95 (2001).
 [14] S. Hilaire and S. Goriely, Nucl. Phys. **A779**, 63 (2006).
 [15] M. Sin *et al.*, in *Proceedings of the International Conference on Nuclear Data for Science and Technology, 22–27 April 2007, Nice, France*, edited by F. Gunsing, E. Bauge, R. Jacqmin, S. Leray, and O. Bersillon (EDP Sciences, Les Ulis, France, 2008), p. 313.
 [16] A. Bohr, Mat. Fys. Medd. K. Dan. Vidensk. Selsk. **26**, 14 (1952).
 [17] M. R. Schmorak *et al.*, Phys. Rev. Lett. **24**, 1507 (1970).
 [18] G. Coleman and R. A. Meyer, Phys. Rev. C **13**, 847 (1976).
 [19] S. Lunardi *et al.*, Phys. Rev. Lett. **53**, 1531 (1984).
 [20] R. A. Gatenby *et al.*, Phys. Rev. C **41**, R414 (1990).
 [21] H. J. Wollersheim *et al.*, Z. Phys. A **341**, 137 (1992).
 [22] T. Belgia *et al.*, Phys. Rev. C **52**, R2314 (1995).
 [23] L. Bargioni *et al.*, Phys. Rev. C **51**, R1057 (1995).
 [24] M. Wilhelm, E. Radermacher, A. Zilges, and P. von Brentano, Phys. Rev. C **54**, R449 (1996); M. Wilhelm, S. Kasemann, G. Pascovici, E. Radermacher, P. von Brentano, and A. Zilges, *ibid.* **57**, 577 (1998).
 [25] C. Fahlander *et al.*, Phys. Lett. **B388**, 475 (1996).
 [26] P. E. Garrett *et al.*, Phys. Rev. Lett. **78**, 4545 (1997).
 [27] R. Schwengner *et al.*, Nucl. Phys. **A620**, 277 (1997).
 [28] R. Georgii *et al.*, Phys. Lett. **B351**, 82 (1995); Nucl. Phys. **A592**, 307 (1995).
 [29] V. Soloviev and L. A. Malov, Nucl. Phys. **A196**, 433 (1972).
 [30] V. Soloviev, A. V. Sushkov, and N. Yu. Shirikova, Int. J. Mod. Phys. E **6**, 437 (1997).
 [31] R. K. Sheline *et al.*, Czech. J. Phys. **49**, 1047 (1999).
 [32] P. E. Garrett *et al.*, J. Phys. G **31**, 1855 (2005).
 [33] M. Pignatelli *et al.*, Nucl. Phys. **A540**, 26 (1992).
 [34] D. G. Burke, Phys. Rev. Lett. **73**, 1899 (1994).
 [35] H. Gruppelaar, P. Nagel, and P. E. Hodgson, Riv. Nuovo Cimento **9**, 1 (1986).
 [36] E. Gadioli and P. E. Hodgson, *Pre-equilibrium Nuclear Reactions* (Oxford University Press, New York, 1992).
 [37] A. J. Koning and M. C. Duijvestijn, Nucl. Phys. **A744**, 15 (2004).
 [38] S. Goriely, M. Samyn, and J. M. Pearson, Phys. Rev. C **75**, 064312 (2007).
 [39] G. Audi, A. H. Wapstra, and C. Thibault, Nucl. Phys. **A729**, 337 (2003).
 [40] T. Belgia *et al.*, *Handbook for Calculations of Nuclear Reaction Data, RIPL-2*, IAEA-TECDOC-1506 (IAEA, Vienna, 2006).
 [41] S. Goriely and J. M. Pearson, in *Proceedings of the International Conference on Nuclear Data for Science and Technology, 22–27 April 2007, Nice, France*, edited by F. Gunsing, E. Bauge, R. Jacqmin, S. Leray, and O. Bersillon (EDP Sciences, Les Ulis, France, 2008), p. 203.
 [42] S. Bjorholm and E. Lynn, Rev. Mod. Phys. **52**, 866 (1980).
 [43] G. Hansen and A. S. Jensen, Report No. BNL-NCS-51694, 1983.
 [44] L. Bonneau, P. Quentin, and D. Samsøen, Eur. Phys. J. A **21**, 391 (2004).
 [45] J.-P. Delaroche, M. Girod, H. Goutte, and J. Libert, Nucl. Phys. **A771**, 103 (2004).
 [46] S. Goriely, S. Hilaire, A. J. Koning, M. Sin, and R. Capote, Phys. Rev. C (submitted).
 [47] A. Schiller *et al.*, Phys. Rev. C **63**, 021306(R) (2001).
 [48] E. Melby *et al.*, Phys. Rev. C **63**, 044309 (2001).
 [49] A. Voinov *et al.*, Phys. Rev. C **63**, 044313 (2001).
 [50] S. Siem *et al.*, Phys. Rev. C **65**, 044318 (2002).
 [51] M. Guttormsen *et al.*, Phys. Rev. C **68**, 064306 (2003).
 [52] A. Schiller *et al.*, Phys. Rev. C **68**, 054326 (2003).
 [53] U. Agvaaluvsan *et al.*, Phys. Rev. C **70**, 054611 (2004).
 [54] R. Chankova *et al.*, Phys. Rev. C **73**, 034311 (2006).

- [55] A. C. Larsen *et al.*, Phys. Rev. C **73**, 064301 (2006).
- [56] S. Goko *et al.*, Phys. Rev. Lett. **96**, 192501 (2006).
- [57] A. J. Koning, S. Hilaire, and M. C. Duijvestijn, in *Proceedings of the International Conference on Nuclear Data for Science and Technology, 22–27 April 2007, Nice, France*, edited by F. Gunsing, E. Bauge, R. Jacqmin, S. Leray, and O. Bersillon (EDP Sciences, Les Ulis, France, 2008), p. 211.
- [58] EXFOR library, <http://www-nds.iaea.or.at/exfor>.
- [59] Z. Y. Bao *et al.*, At. Data Nucl. Data Tables **75**, 1 (2000).